AD-A190 002 XDP (EXPENDABLE DISSIPATION PROFILER) MECHANICS(U) 1/1
NAVAL OCEAN RESEARCH AND DEVELOPMENT ACTIVITY NSTL
STATION MS K D SAUNDERS ET AL. 1983

UNCLASSIFIED F/G 8/3 NL

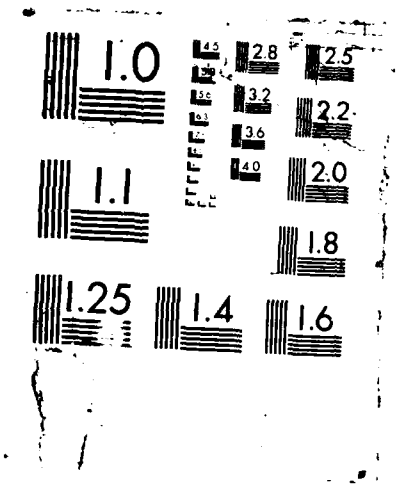
1.0
2.8
2.5
3.2
2.2
3.6
4.0
2.0
1.1
1.8
1.25
1.4
1.6

XDP MECHANICS

Kim David Saunders[1] and Linda Knauer[2]

[1] Naval Ocean Research and Development Activity
NSTL, MS 39529-5004

[2] Planning Systems Inc.
115 Christian Lane, Slidell, LA 70458

ABSTRACT

Interaction between the oceanic vertical shear field and the natural response of a recently developed expendable dissipation profiler (XDP) causes errors to be introduced in small scale velocity measurements. A numerical model was developed to study this problem and two sources of errors were determined, the primary source being the shear induced torques at the instrument length scale.

1. INTRODUCTION

The direct measurement of the dissipation rate of small scale turbulence has long been a goal of oceanographers, but has become feasible only in recent years with the development of probes capable of measuring shears on subcentimeter scales. The primary sensor for this type of measurement is the air-foil shear probe, initially developed by Ribner and Siddon (1969, *cited in Osborne and* Crawford, 1978) and subsequently improved for water operation by Osborne and Crawford (1978).

The airfoil probe operates on the principle that an ogive, passing at constant velocity though a flow field with shear at right angles to its motion, will experience a lift force which is a function of the shear field and its velocity. If the ogive is elastic, it will deform in a manner nearly proportional to that lift force. The actual probes are constructed by mounting a beam of piezoelectric material in a silicone rubber ogive that is mounted on the end of a long "sting" at the front of the vehicle.

The silicone rubber is compliant and imparts any deformation to the beam, the electrical output of which is amplified and filtered by the circuitry in the vehicle. The data may be stored internally in the vehicle as in the Camel (Osborn, 1977); or they may be sent to the surface via a direct data link as in the Advanced Microstructure Profiler (AMP) (Gregg, 1982) or the expendable dissipation profiler (XDP).

The XDP was designed and built by Lueck and Osborn (1983) as a relatively inexpensive expendable probe to measure dissipation from a moving vessel. The basic design of the vehicle is similar to the well-known XBT, with certain differences that were introduced to reduce the mechanical vibration of the instrument.

One phase of the Ocean Measurement Sensors Project at NORDA has been the evaluation of XDPs. In November, 1984, 12 XDPs were deployed during the TROPIC HEAT cruise of the University of Washington Applied Physics Laboratory. Each of the XDPs was dropped immediately after UW/APL had completed an AMP (Advanced Microstructure Profiler) drop.

The AMP (Gregg, 1982) has two airfoil turbulence probes in its sensor suite. The AMP vehicle is longer and more massive than the XDP vehicle and is expected to provide a much more stable platform from which to measure turbulent velocity fluctuations. This is confirmed by the excellent agreement with the Nasmyth spectral form (Oakey, 1983) for the observed level of dissipation (obtained from integrating the shear spectrum).

When the records from both instruments were compared, the XDP showed much larger apparent dissipation rates than those obtained from the AMP. The XDP spectra often were found to have unexpected peaks in 1 to 10 cpm wavenumber range and an excess of variance at high wavenumbers over the Nasmyth spectra for the same integrated shear variance. A typical spectrum of the XDP shear data is illustrated in figure 1.

If the XDP is to be used as a reliable instrument for turbulence measurements, the cause of the differences between the AMP and XDP measurements must be located and corrected. Because some of the peaks occurred in the 1 to 10 cpm band, we suspected that the background shear field might be amplified by the natural modes of oscillation of the XDP vehicle at scales near the vehicle length.

It is difficult and expensive to design and conduct an experiment to measure the amplification of the actual shear field in the ocean by an XDP. A numerical simulation offers a simpler means of testing this hypothesis and provides additional information that could not be obtained as regards the mechanics of the XDP vehicle without a major engineering effort.

2. METHOD

The basic method followed in performing this simulation is to model the motion of an XDP vehicle by applying Newton's third law in two degrees of translation and one of rotation to the XDP body. The major problem in simulating the motion of the vehicle is to obtain a good representation of the

CH2498-4/87/0000- 200 $1.00 © 1987 IEEE

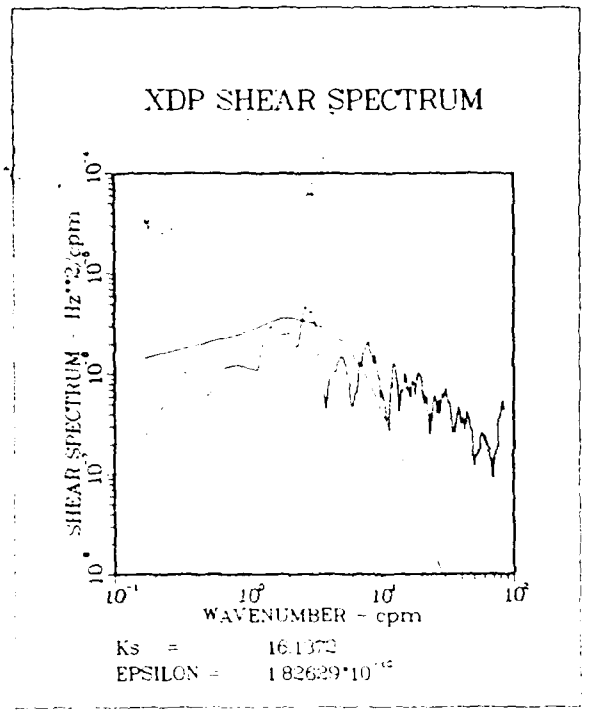

Figure 1. Spectrum of XDP shear data obtained during the Tropic Heat cruise of November, 1984. The data used for this spectrum were from record XDPTH01C, data points 10000-13500, using Hanning windowing and 50% overlap. The dissipation rate was computed by integrating to the cutoff wavenumber, Ks. Ks, a function of dissipation rate, was obtained by iteration. The superposed curve is the Nasmyth spectrum for the estimated dissipation rate.

forcing field: the detailed velocity structure of the ocean as a function of depth.

In this model, the vehicle is constrained to planar motion. This assumption was made both for computational simplicity and ease of interpretation of the results. The other main assumption was the value of the virtual mass and moments of inertia. The virtual mass was taken as the sum of the vehicle mass and that of the water displaced by the vehicle. The virtual moment of inertia was taken as the sum of the vehicle moment of inertia about the center of gravity and the moment of inertia of the displaced water. The coordinate system for the instrument model is shown in figure 2.

3. INSTRUMENT CHARACTERISTICS

The XDP is similar in shape to an XBT. It has a fine nose section to provide a center of gravity below the center of buoyancy as in the XBT. The major differences between the XDP and the XBT vehicle are 1) the long "wing" at the nose of the XDP at the end of which is mounted the airfoil probe and along the side of which is mounted the thermistor, 2) the lack of fins (replaced by a four rubber rings to provide drag and prevent

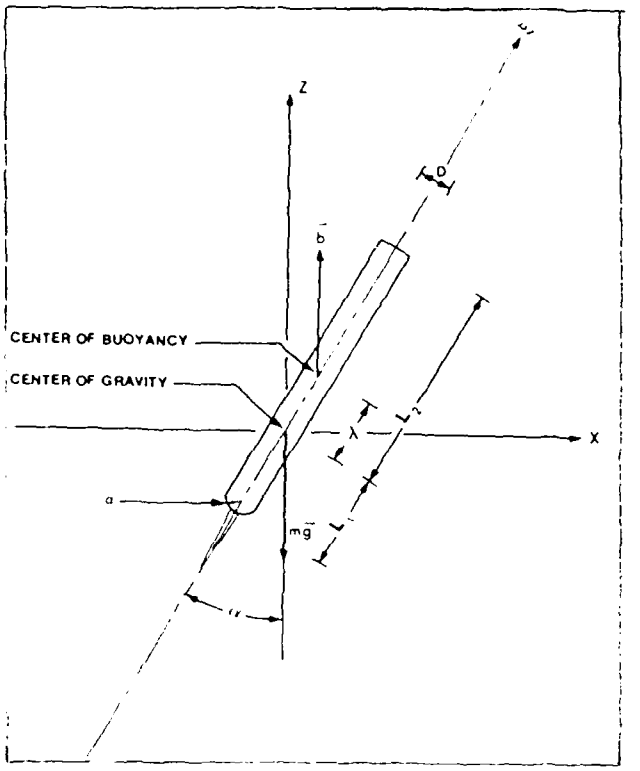

Figure 2. Coordinate system for XDP vehicle. The angle α is taken positive in the counterclockwise sense. The origin for ξ is the center of gravity (mass) of the XDP vehicle.

rotation), and 3) the inside-out winding of the wire coil.

The physical dimensions and properties of the vehicle are summarized in table 1, along with other constants used in the numerical simulation.

The mass of the vehicle was determined by weighing the XDP on a laboratory balance. The moment of inertia was determined by mounting the XDP as a compound pendulum and measuring the period (Timoshenko and Young, 1940, p 401). The moment of inertia about the center of gravity was computed by the usual formula (loc. cit., p 508).

4. DIFFERENTIAL EQUATIONS

The model differential equations are derived from Newton's third law, balancing mass times acceleration in the horizontal and vertical directions and the angular momentum form of the third law for rotation in the y = 0 plane. In all this work, the motion of the instrument is assumed to be constrained to one plane (y = 0). The coordinate system is defined in the (x,z) plane with z taken positive upward. We can symbolically write the differential equations of motion as

$\dot{z}$ = w = vertical velocity,

$\dot{x}$ = u = horizontal velocity,

$\dot{\alpha} = \dot{\psi}$ = angular velocity ,

$\dot{w}$ = gravitational accceleration + buoyancy acceleration + drag acceleration,

$\dot{u}$ = horizontal drag acceleration,

$\dot{\psi}$ = gravitational restoring torque + shear torque

The specific formulation of these accelerations is given as

$$\dot{w} = m_v^{-1} [- mg + b - \rho C_D^L (\pi a^2 + LD | \sin\alpha |) w|w|]$$

$$\dot{u} = m_v^{-1} C_D^L \rho D L (U(z) - u)|U(z) - u|$$

$$\dot{\psi} = - b\lambda I_v^{-1} \sin\alpha - I_v^{-1} \int_{-L_1}^{L_2} \xi(\cos\alpha\, Q^{(x)} + \sin\alpha\, Q^{(z)})\, d\xi,$$

where

$$Q^{(x)} = 0.5\, C_D^L \rho \cos\alpha\, [U(z+\xi\cos\alpha)-u] |U(z+\xi\cos\alpha)-u| D(\xi),$$

$$Q^{(z)} = -0.5\, C_D^L \rho D(\xi)\, w\, |w| \sin\alpha .$$

Background shear field, U(z)

The driving force for this set of differential equations is provided by the effect of the background horizontal velocity field, U(z) exerting a drag force on the XDP vehicle. The velocity field was estimated by constructing a depth series of shear based on the Garget, et al. (1980) model shear spectrum. The specific spectrum used was given by:

$$S(k) = C_0 , \quad k < k_0 = 0.1\ m^{-1} ,$$

$$= C_0 (k/k_0)^{-1} , \quad k_0 < k < k_1 = 1\ m^{-1},$$

= Nasmyth Spectrum, $k > k_1$;

$$C_0 = (N/N_0)^2 \times 2 \times 10^{-4}\ s^{-2}/cpm ;$$

$$N_0 = 1.4\ cph .$$

In the range $k > 1\ m^{-1}$, the Nasmyth spectrum (Oakey, 1983) was used with a dissipation rate of $\varepsilon = 1 \times 10^{-6}$ W/kg.

TABLE 1

Variable	Description	Base Value
α	Angle of XDP vehicle to the vertical, positive in counterclockwise sense	
a	Radius of XDP nose	0.025 m
b	Buoyancy	1.6 N
C_D^L	Transverse drag coefficient	1.0
D	Diameter of instrument	0.05 m
g	Acceleration of gravity	9.8 m s^{-2}
I_v	Virtual Moment of Inertia	0.0156 kg m^2
L	Total length of XDP	0.340 m
L_1	Distance CG to nose	0.097 m
L_2	Distance CG to tail	0.243 m
λ	Distance CG to center of buoyancy	0.073 m
m	Mass of XDP	1.088 kg
m_v	Virtual Mass	2.176 kg
ρ	Density of Seawater	1025 kg m^{-3}
S(k)	Shear Spectrum	
u	Horizontal XDP velocity	
U(z)	Background velocity field	
w	Vertical XDP velocity	
x	Horizontal XDP position	
z	Vertical XDP position	
ψ	Angular velocity of XDP	
ξ	Integration variable (Distance from center of gravity, positive aft)	

The model shear field was constructed by taking the square root of the spectrum, multiplying it by a complex factor $\exp[i\phi(k)]$, where $\phi(k)$ is a random variable, uniformly distributed over $(0,2\pi)$.

An inverse Fourier transform was then applied to the resultant function of k to get random phase shear profile. The shear profile was then integrated numerically to obtain the velocity profile.

Symbolically (in continuous form):

$$U(z) = \int_0^z F_\zeta^{-1}(S^{1/2}(k) \exp[\, i\phi(k)\,]\,)\, d\zeta,$$

where

$$F_\zeta^{-1}\{f(k)\} = (2\pi)^{-1} \int_{-\infty}^{\infty} f(k) \exp(ik\zeta)\, dk$$

is the inverse Fourier transform.

A 65536 point discrete Fourier transform was used providing a 1 cm spacing of points. As the aperture of the probe was about 2 cm, this was felt to be sufficient to model the response of the probe. For the rotational torque calculations, this spacing gave about 34 points for integrating the forces over the length of the vehicle.

5. DISCUSSION

Forcing mechanisms

Two mechanisms should affect the motion of the vehicle. Both produce torques on the vehicle body which will cause it to oscillate as it falls through the water column and thus induce spurious additions to the observed transverse current field. The first and most obvious torque is caused by the shear field of the background flow. This field will, in general, induce a torque because a varying distribution of force will be applied to the body along its length.

The source of the second torque is not as obvious. If the vehicle were to fall into a region of constant flow, there would be a uniform force over the whole vehicle due to the difference in the horizontal velocity component of the vehicle and the background flow. In most free fall vehicles, the center of gravity (mass) is below the center of projected transverse area of the vehicle and, as the moment of force is computed about the center of gravity, a uniform force distribution will result in a torque. Thus, at low frequencies (and wavenumbers), we should expect to see the angle of the vehicle correlated with the background horizontal velocity. This will not cause problems with induced velocities, due to the low frequency of the motions, but will cause an error due to the angular sensitivity of the probe (not modeled in this study).

Model Results

The differential equations were integrated using the IMSL version of the Gear solver for stiff ordinary differential equations (IMSL, 1982). The initial conditions on all variables were set to zero, so only the external forcing would affect the motion of the XDP vehicle.

The velocity and shear field used to drive the probe motion are plotted as a function of depth in figures 3 and 4. Figure 5 presents the horizontal motion of the probe with depth; figure 6, the horizontal velocity; figure 7, the rotational angle; figure 8, the angular velocity; and figure 9, the vertical fall rate. The "sensed" horizontal velocity was computed by combining the velocity due to rotation with the difference in horizontal motion of the vehicle and the background flow:

$$U_{sensed} = U(z) - u - L_1\psi .$$

For this study, no attempt has been made to model the dynamic response of the probe. There should be little disagreement between the sensed flow as computed above and the sensed flow after applying the probe's low pass response filter for the scales under consideration as the probe cutoff wavenumber is about 1 cm.

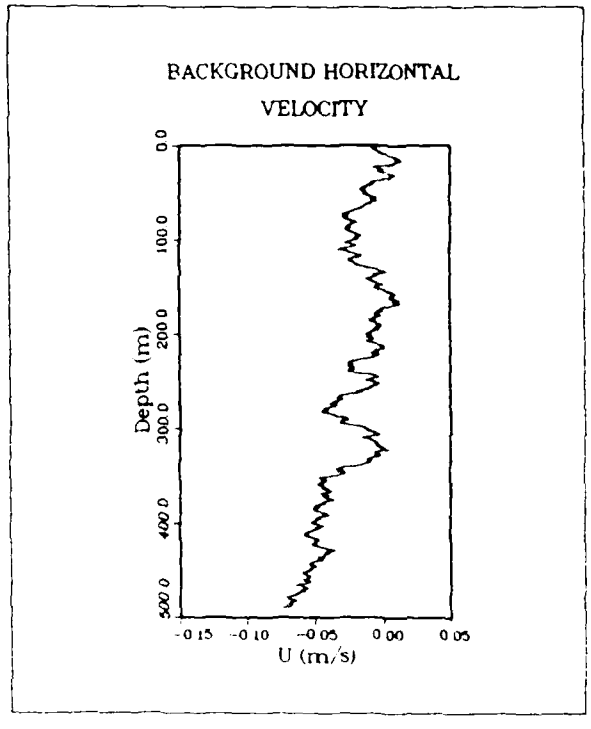

Figure 3. Background horizontal velocity versus depth. The velocity was obtained by integrating the model shear field.

The "sensed" velocity is plotted versus depth in figure 10 . When this figure is compared with figures 3 and 8, it appears that the $L_1\psi$ component of the "sensed" velocity is nearly as important as the U(z) component. The scale of the plot makes it difficult to see the details of the vehicle motion effects on the "sensed" velocity.

To determine the contributions of the vehicle oscillations on the observed velocities and the time/space scales at which effects occur, spectra of both the "sensed" velocity and the background velocity were computed. These spectra were computed

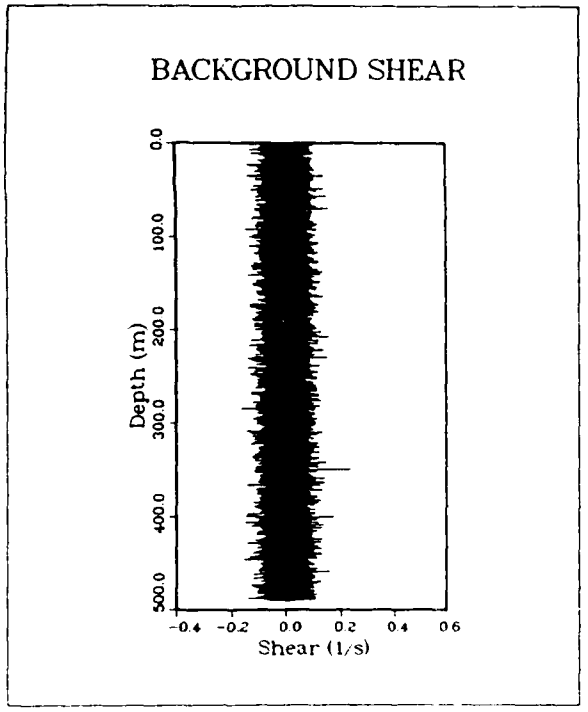

Figure 4. Background vertical shear field versus depth. The shear field was obtained from the inverse Fourier transform of the Garrett, et al. (1980) model oceanic shear spectrum.

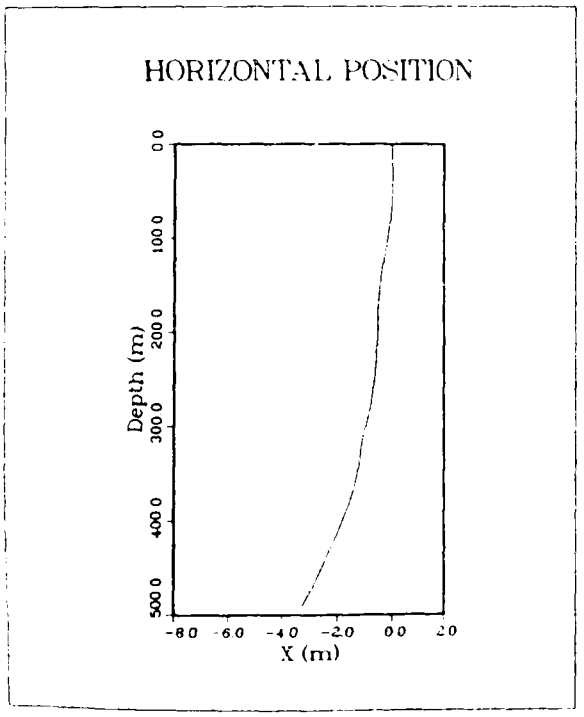

Figure 5. Horizontal position of probe versus depth.

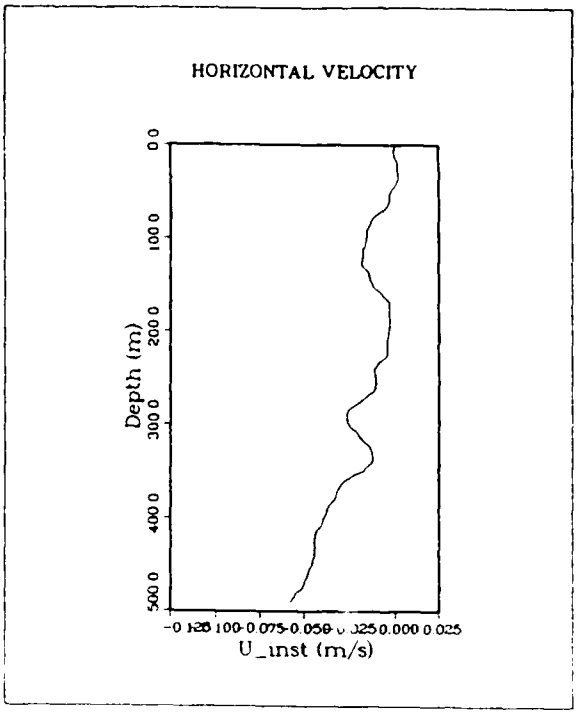

Figure 6. Horizontal velocity of probe versus depth.

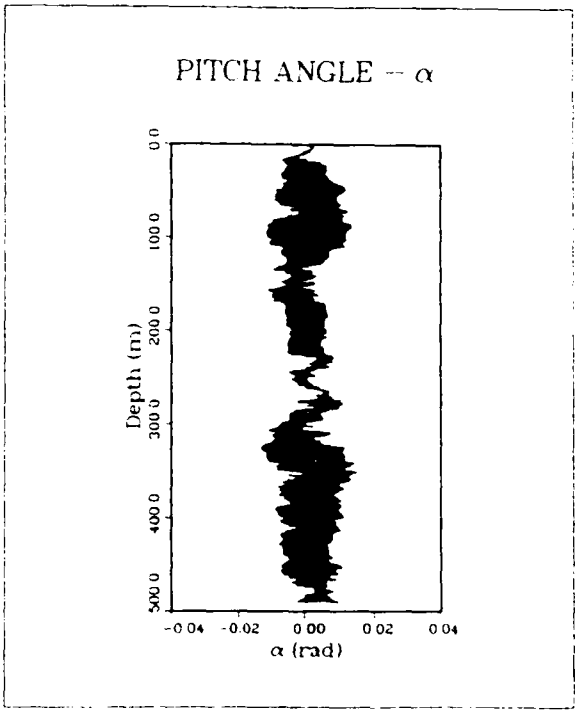

Figure 7. Rotational angle versus depth. The medium frequency oscillations are obscured on the scale of the plot.

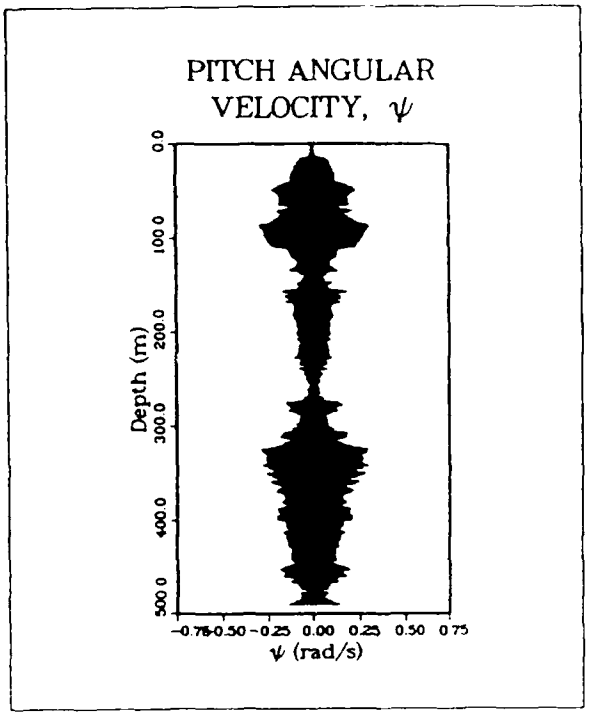

Figure 8. Angular velocity versus depth. The medium frequency oscillations, obscured by the scale of the plot contribute significantly to the "sensed" velocity.

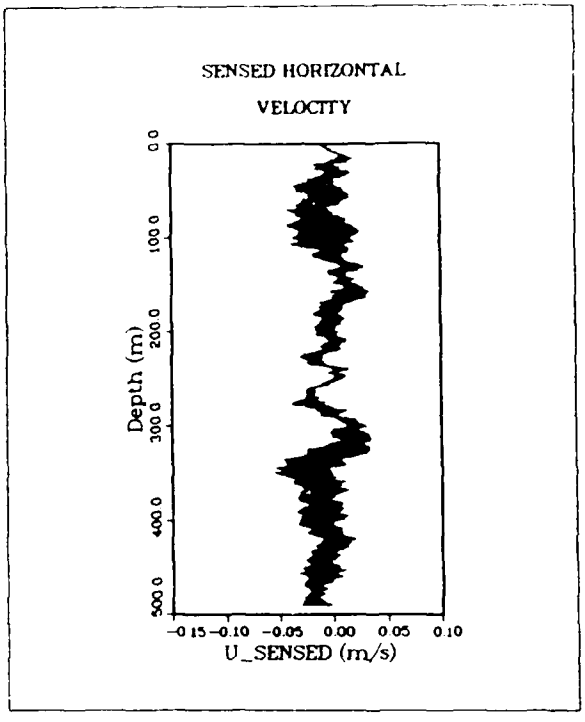

Figure 10. "Sensed" velocity at probe versus depth. Only the motion at the probe was modeled. The probe response was not modeled.

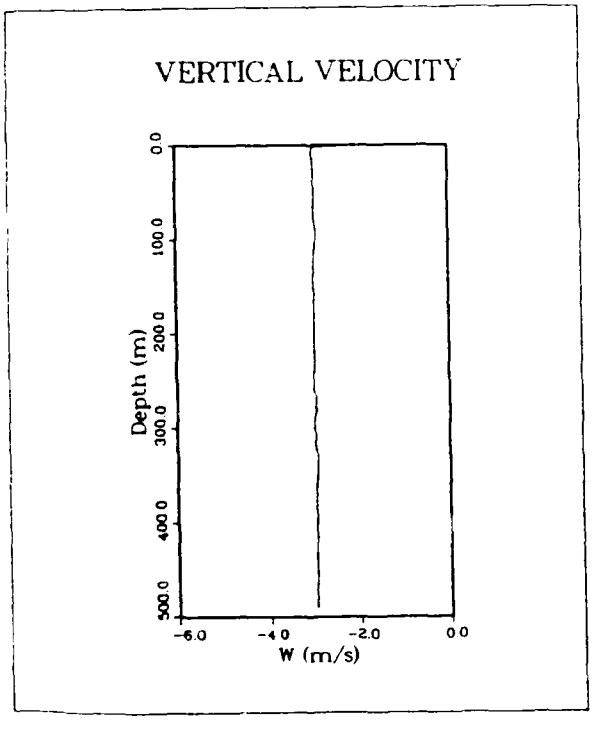

Figure 9. Fall rate versus depth. The probe reaches a nearly constant fall rate of about 3 m/s within 1 m of being dropped from rest.

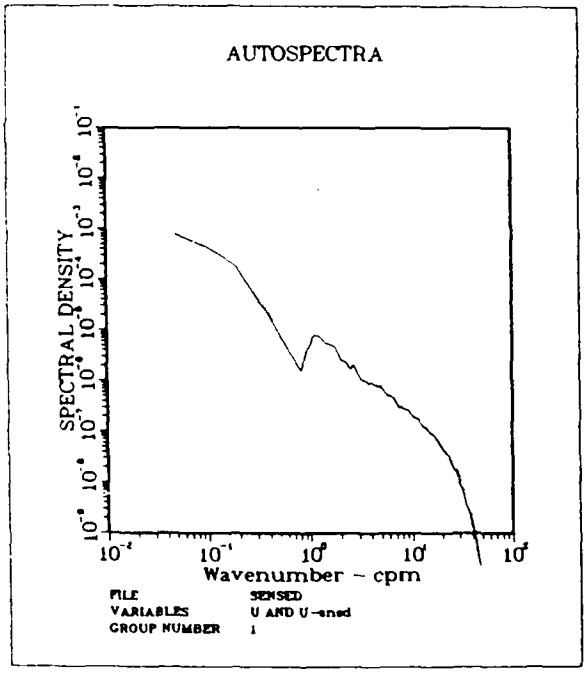

Figure 11. Spectra of U(z) and $U_{sensed}(z)$ as functions of wavenumber. The spectral levels of the sensed velocities transverse to the probe at well reproduced for wavelengths greater than 4 m and less than 20 cm.

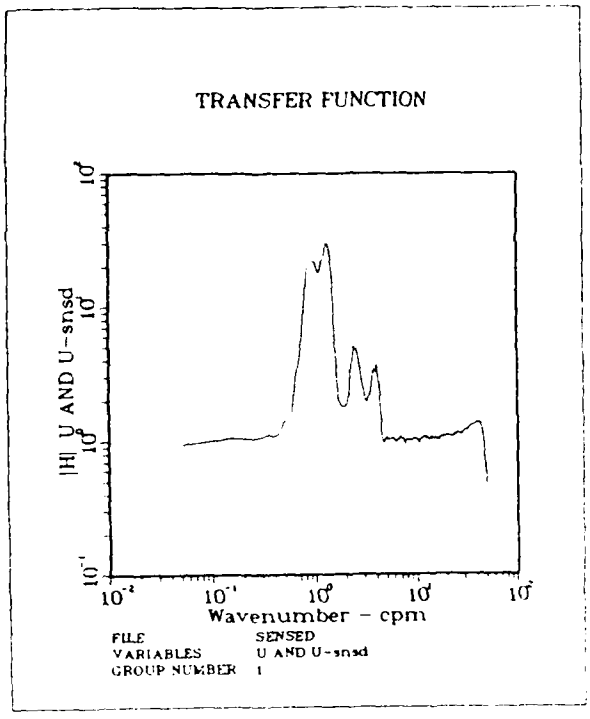

Figure 12. Transfer function between U(z) and $U_{sensed}(z)$. The sensed velocities are amplified with respect to the background velocities in the 0.4 to 5 cpm wavenumber band. The maximum amplification occurs at about 1.3 cpm with a 30 fold amplification.

for times and depths after which the probe had reached terminal velocity (about 1 to 3 meters). These spectra are plotted in figure 11. As can be seen, the "sensed" velocity field has a very strong peak in the 1 to 10 cpm band, indicating a very strong amplification of the background shear, as was hypothesized. The transfer function amplitude which is equal to the ratio of the output spectrum to the input spectrum was also computed and is depicted in figure 12. This figure shows that the background field is amplified by about a factor of 5 - 10 in the 1 to 10 cpm band.

The numerical simulation was repeated for several different values of ε ranging from 10^{-6} W/kg to 10^{-10} W/kg to determine the effect of varying dissipation rates on the degree of amplification. These effects indicate a weak non linearity: the amount of amplification increases weakly with the dissipation rate.

Unresolved Problems

While this numerical study has shown that the probe's response significantly affects the observed shear in the 1 - 10 cpm band, it has not clarified the reasons for the large apparent differences in observed dissipation rates obtained from the XDP and the AMP. Dr. A.W. Green, NORDA, personal communication, has suggested that some of the observed peaks in the low frequency band (1 - 10 cpm) may be due to slow rotations of the vehicle coupled with precessional modes of oscillation. The high frequency flattening of the spectrum may be due, in part, to despooling noise associated with the signal wire and to wake noise transmitted through the instrument to the sensor element.

6. CONCLUSIONS

While several observations of the XDP probe's behavior that are still unaccounted for, this modeling study has shown that there may be considerable amplification of the background shear field in the wavenumber band between 1 and 10 cpm. This is the same band where the peak in turbulent energy dissipation is expected to occur (based on the Nasmyth spectrum). Neglect of the probe response in this region will cause serious errors in estimation of the dissipation rate. Correction of the amplification effect is made more difficult by the nonlinearity of the effect, the occurrence of spectral peaks not predicted by the model and high frequency flattening of the spectrum. It appears that further work is required before the expendable dissipation profiler is ready to be used as a routine survey tool.

REFERENCES

Gargett, A.E., P.J. Hendricks, T.B. Sanford, T.R. Osborn and A.J. Williams,III 1980. A Composite Spectrum of Vertical Shear in the Upper Ocean from the Profilers EMVP, SCIMP and CAMEL. Pacific Marine Science Report 80-11, Institute of Ocean Sciences, Sidney, B.C.

Gregg, M.C., W.E. Nodland, E.E. Aagaard, and D.H. Hirt 1982. Use of Fiber Optic Cable with a Free-fall Microstructure Profiler. Proc. Oceans '82, 260-265, Marine Technology Society, Washington, D.C.

IMSL 1982. IMSL Library Reference Manual, 1

Lueck, R.G. and T.R. Osborne 1983. Expendable Dissipation Profiler Manual. Naval Postgraduate School. Monterey, CA.

Oakey, N.S. 1983. Determination of the Rate of Dissipation of Turbulent Energy from Simultaneous Temperature and Velocity Shear Measurements. J.Physical Oceanography, 12(3), 257-271.

Osborn, T.R. 1977. The design and performance of free-fall microstructure instruments at the Institute of Oceanography, University of British Columbia. IOUBC Manuscript Report No. 30.

Osborn, T.R. and W.R. Crawford 1978. Turbulent Velocity Measurements with and Airfoil Probe. NATO Advanced Study Institute on Instruments and Methods in Air Sea Interaction

Siddon, T.E. 1965. A Turbulence Probe Utilizing Aerodynamic Lift. University of Toronto, Inst. for Aerospace Studies. Tech. Note 88.

Timoshenko, S., and D.H. Young 1940. Engineering Mechanics, McGraw Hill Book Co., New York.

END

DATE

FILMED

5-88

DTIC